Minimum-Fuel Earth-Based Orbit Transfers Using Multiple-Domain Adaptive Radau Collocation

Brittanny V. Holden* Elisha R. Pager[†] Anil V. Rao[‡]

University of Florida Gainesville, FL 32611-6250

Nomenclature

a = semi-major axis

 A_T = number of thrust arcs

AU = acceleration unit

 c_p = number of initial collocation points in each mesh interval

DU = length unit e = eccentricity

 e_D = desired eccentricity of terminal orbit

 e_f = eccentricity of terminal orbit e_0 = eccentricity of initial orbit

f = second modified equinoctial orbital element

FU = force unit

g = third modified equinoctial orbital element

 g_0 = standard gravitational acceleration

h = fourth modified equinoctial orbital element

i = orbital inclination

 i_D = desired inclination of terminal orbit

 i_f = inclination of terminal orbit i_0 = inclination of initial orbit

 I_{sp} = specific impulse J = cost functional

k = fifth modified equinoctial orbital element

L = true longitude (sixth modified equinoctial orbital element)

N = total revolutions around Earth M = number of initial mesh intervals

m = mass of spacecraft

 m_0 = initial mass of spacecraft

MU = mass unit

^{*}Ph.D. Candidate, Department of Mechanical and Aerospace Engineering, brittannyholden@gmail.com.

[†]Senior Professional Staff, The Johns Hopkins University Applied Physics Laboratory, elisha.pager@gmail.com.

[‡]Professor, Department of Mechanical and Aerospace Engineering, anilvrao@ufl.edu, Associate Fellow AIAA (Corresponding Author).

p = semi-parameter (first modified equinoctial orbital element)

 p_D = desired semi-parameter of terminal orbit

 p_f = semi-parameter of terminal orbit p_0 = semi-parameter of initial orbit

 R_E = radius of Earth

 s_0 = maximum allowable thrust acceleration

t = time

 $t_0 = \text{initial time}$ $t_f = \text{terminal time}$

 $t_T = \text{total time thrusting}$ T = thrust magnitude

TU = time unit

 $T_{\text{max}} = \text{maximum thrust magnitude}$

VU = speed unit u = thrust direction

 $u_n = \text{normal component of thrust direction}$ $u_r = \text{radial component of thrust direction}$ $u_t = \text{transverse component of thrust direction}$

 Δ_n = normal non-two-body perturbations of the spacecraft Δ_r = radial non-two-body perturbations of the spacecraft = transverse non-two-body perturbations of the spacecraft

 ΔV = the total impulse of the spacecraft

 η = threshold to detect the relative size of jumps in the control

 μ_E = gravitational parameter of Earth

 ν = true anomaly

 ω = argument of periapsis

 Ω = longitude of the ascending node

 Ω_0 = longitude of the ascending node of the initial orbit

1 Introduction

Low-thrust orbital transfer is a topic of ongoing interest in the space community. A significant amount of research has been conducted previously on the design of low-thrust orbital transfer missions 11–18. References 11–7 used various forms of direct optimization methods to optimize very-low-thrust orbit transfers. Reference 8 obtained solutions to low-thrust orbit trajectory optimal control problems using genetic algorithm, while Ref. 9 combined artificial neural networks and evolutionary algorithms to create evolutionary neurocontrollers in order to solve low-thrust orbital transfer problems. References 10–12 employed homotopic methods to optimize low-thrust transfers where the thrusting structure may be discontinuous. Reference 13 obtained solutions

to low-thrust orbit trajectory optimal control problems by applying a hybrid optimization method that incorporated a multi-objective genetic algorithm with a low-thrust trajectory optimizer that applies calculus of variations. Reference 14 presents a novel approach to solving low-thrust orbit transfers, where a first-order approximated analytical solution of Gauss planetary equations using direct finite perturbative elements was implemented in the solution process. This method was shown to have lower computational cost and higher accuracy than a second-order explicit numerical integrator. References 15 and 16 solved an optimal control problem of a low-thrust orbit transfer with eclipsing. Reference 17 implemented both indirect and direct methods when solving a minimum-fuel low-thrust Earth-to-Mars orbital transfer. Reference 18 primarily focused on solving hybrid-optimal control problems by conducting a survey on approaches for low-thrust trajectory optimization.

This research is inspired by the work of Ref. 4 and both works consider the problem of LEO-to-MEO, LEO-to-HEO, and LEO-to-GEO low-thrust orbital transfer. It is noted, however, that this research and the work of Ref. 4 differ in the following ways. First, in this research the thrusting structure is determined as part of the solution process whereas Ref. 4 assumed a priori a burn-coast-burn thrusting structure based on the work of Ref. 19. Second, in order to determine the thrusting structure, a recently developed bang-bang and singular optimal control (BBSOC) method 20 is employed using multi-domain Legendre-Gauss-Radau (LGR) collocation as implemented in the MATLAB optimal control software GPOPS — II 21. It is important to note that, because the thrusting structure is not assumed a priori, the performance (that is, the minimum-impulse) obtained in this study shows a significant improvement over the performance obtained in Ref. 4 and this improvement increases as the maximum thrust acceleration decreases. Third, the improved performance obtained in this study leads to a thrusting structure that differs significantly from the burn-coast-burn thrusting structure assumed in Ref. 4. Fourth, the thrusting structure obtained for the various types of orbital transfer (LEO-to-MEO, LEO-to-HEO, and LEO-to-GEO) is shown

for particular cases of maximum allowable thrust acceleration and provide improved insight into the optimal thrusting structure for such transfers.

This paper is organized as follows. Section 2 presents the one-phase minimum-fuel Earth-based orbital transfer optimal control problem by providing the modeling assumptions, dynamics, path constraints, event constraints, the units used to solve the problem, boundary conditions, and variable bounds. Section 3 presents the procedure on how to create the initial guess for each problem case. Section 4 describes the bang-bang and singular optimal control (BBSOC) method used to solve the orbital transfer problems in this paper. Section 5 shows the key results obtained in this study and provides a discussion of these results. Finally, Section 6 provides conclusions on this research.

2 Problem Description

2.1 Equations of Motion

The differential equations of motion for the spacecraft under central body gravitation are given in terms of modified equinoctial elements (MEE) as [22]

$$\frac{dp}{dt} = \sqrt{\frac{p}{\mu_E}} \frac{2p}{w} \Delta_t,$$

$$\frac{df}{dt} = \sqrt{\frac{p}{\mu_E}} \left[\sin L \Delta_r + \frac{1}{w} \left[(w+1)\cos L + f \right] \Delta_t - \frac{g}{w} \left(h \sin L - k \cos L \right) \Delta_n \right],$$

$$\frac{dg}{dt} = \sqrt{\frac{p}{\mu_E}} \left[-\cos L \Delta_r + \frac{1}{w} \left[(w+1)\sin L + g \right] \Delta_t + \frac{g}{w} \left(h \sin L - k \cos L \right) \Delta_n \right],$$

$$\frac{dh}{dt} = \sqrt{\frac{p}{\mu_E}} \frac{q^2}{2w} \cos L \Delta_n,$$

$$\frac{dk}{dt} = \sqrt{\frac{p}{\mu_E}} \frac{q^2}{2w} \sin L \Delta_n,$$

$$\frac{dL}{dt} = \sqrt{\frac{p}{\mu_E}} \left(\frac{w}{p} \right)^2 + \frac{1}{w} \sqrt{\frac{p}{\mu_E}} \left(h \sin L - k \cos L \right) \Delta_n,$$

$$\frac{dm}{dt} = -\frac{T}{g_0 I_{sp}},$$
(1)

where

$$(p, f, g) = (a(1 - e^{2}), e\cos(\omega + \Omega), e\sin(\omega + \Omega)),$$

$$(h, k, L) = (\tan(i/2)\cos\Omega, \tan(i/2)\sin\Omega, \Omega + \omega + \nu),$$

$$q^{2} = 1 + h^{2} + k^{2},$$

$$w = 1 + f\cos L + g\sin L,$$

$$(2)$$

$$(\Delta_r, \Delta_t, \Delta_n) = \frac{T}{m}(u_r, u_t, u_n).$$

where $\mathbf{\Delta} = (\Delta_r, \Delta_t, \Delta_n)$, are the radial, transverse, and normal components of the thrust acceleration, $\mathbf{\Delta}$. The control consists of the thrust magnitude, T, and the thrust direction, $\mathbf{u} = (u_r, u_t, u_n)$, where u_r is the component along the direction of the position, \mathbf{r} , where \mathbf{r} is measured from the center of the Earth to the spacecraft, u_n is the component along the specific angular momentum, $\mathbf{h} = \mathbf{r} \times \mathbf{v}$ (where \mathbf{v} is the inertial velocity of the spacecraft), and u_t is the component along the direction $\mathbf{h} \times \mathbf{r}$. Next, in order to ensure that the thrust direction is a unit vector, the control equality path constraint

$$\mathbf{u} \cdot \mathbf{u} = u_r^2 + u_t^2 + u_n^2 = 1 \tag{3}$$

is enforced to guarantee that the thrust direction is a unit vector. It is noted that the thrust direction is parameterized using Cartesian variables because any Cartesian triplet (u_r, u_t, n) defines a unique direction in three-dimensional space. Finally, the following initial and terminal boundary conditions (event constraints) are enforced in order to ensure that the spacecraft starts and terminates in the desired orbits [23]:

$$\begin{aligned}
\left[p, f^2 + g^2, h^2 + k^2, \tan^{-1}(k, h)\right]_{t=t_0} &= \left(a_0(1 - e_0^2), e_0^2, \tan^2(i_0/2), \Omega_0\right), \\
\left[p, f^2 + g^2, h^2 + k^2\right]_{t=t_f} &= \left(a_f(1 - e_f^2), e_f^2, \tan^2(i_f/2)\right),
\end{aligned} (4)$$

where $\tan^{-1}(y, x)$ is the four-quadrant inverse tangent. It is noted in Eq. (4) that a_0 , e_0 , i_0 , Ω_0 , a_f , e_f , and i_f are parameters determined by the initial and terminal orbits as given in Table 2. The numerical values of the physical constants and physical parameters used to solve the problems under consideration in this paper are given in Table 1.

Table 1: Physical constants.

Quantity	Value
R_E	$6.378145 \times 10^6 \text{ m}$
μ_E	$3.986004418 \times 10^{14} \text{ m}^3 \cdot \text{s}^{-2}$
g_0	$9.80665 \text{ m} \cdot \text{s}^{-2}$
m_0	$1.000\times10^3~\mathrm{kg}$
I_{sp}	$1.000\times10^3~\mathrm{s}$

2.2 Boundary Conditions and Bounds

Table 2 presents the orbital elements of the initial low-Earth orbit and terminal medium-Earth, high-Earth, or geosynchronous orbits 4. Next, lower and upper limits on the components of the

Table 2: Orbital elements for the initial and terminal orbits.

Orbital Element	LEO	MEO	HEO	GEO
Semi-major Axis, a (km)	7,003	26,560	26,578	42,287
Eccentricity, e	0	0	0.73646	0
Inclination, i (deg)	28.5	54.7	63.435	0
Longitude of the Ascending Node, Ω (deg)	0	Free	Free	Undefined
Argument of Periapsis, ω (deg)	Undefined	Undefined	Free	Undefined
True Anomaly, ν (deg)	Free	Free	Free	Free

state and control are shown in Table 3. Furthermore, all initial and terminal boundary conditions on the state are free except the following that are fixed: $(t_0, p(t_0), m(t_0), p(t_f)) = (0, p_0, m_0, p_f)$, where p_0 and p_f correspond to the initial and terminal semi-parameter, respectively, where $p = a(1 - e^2)$. Finally, Table 4 gives the maximum allowable thrust acceleration, s_0 , and the maximum thrust magnitude, T_{max} , for all cases studied in this research 4.

Table 3: Lower and upper bounds.

Variable	[Lower, Upper]
T	$[0,T_{\rm max}]$
f	[-1, +1]
g	[-1, +1]
h	[-1, +1]
k	[-1, +1]
m	$[0.01*m_0, m_0]$

Table 4: Maximum allowable thrust acceleration and maximum thrust values for all cases.

Case	$s_0 \left(\mathbf{m} \cdot \mathbf{s}^{-2} \right)$	$T_{\max}\left(\mathbf{N}\right)$
1	10	10000
2	5	5000
3	1	1000
4	0.5	500
5	0.1	100
6	0.05	50
7	0.01	10

2.3 Optimal Control Problem

The optimal control problem for the various Earth orbit transfers is stated as follows. Determine the state (p, f, g, h, k, L, m), control (T, u_r, u_t, u_n) , and terminal time t_f which maximizes the final mass of the spacecraft, $m(t_f)$. For that reason, the following cost functional needs to be minimized

$$J = -m(t_f) \tag{5}$$

while satisfying the dynamics and constraints in Section [2.1] along with the variable bounds and boundary conditions in Section [2.2].

3 Initial Guess Generation

This section explains how initial guesses required by the general-purpose MATLAB optimal control software GPOPS — II [21] are generated to solve the single-phase minimum-fuel Earth-based orbit transfer optimal control problem described in Section [2]. Two distinct initial guess generation methods are described in Section [3.1] and Section [3.2]. The first initial guess generation method is used for maximum allowable thrust acceleration values that lead to solutions that are less than one orbital revolution (that is, a partial orbital revolution) while the second initial guess generation method is used for maximum allowable thrust acceleration values that lead to solutions that are more than one orbital revolution (that is, multiple orbital revolutions). In order to determine which generation method is applied, each case of the optimal control problem is solved on the GPOPS — II default initial mesh (that is, no mesh refinement is implemented) with the initial guess generation method described in Section [3.1] to determine if the optimal solution is categorized as either a partial orbital revolution or a multiple orbital revolution solution. If the solution is a partial orbital revolution, then the optimal control problem is solved using the guess generation method in Section [3.1]. On the other hand, if the solution consists of multiple orbital revolutions, then the optimal control problem is solved using the generation method in Section [3.2].

3.1 Initial Guess for Partial Orbital Revolution Solutions

For the problem cases categorized as partial orbital revolution solutions, the ordinary differential equations solver ode113 in MATLAB is used to generate the initial guess. The ODE solver integrates the spacecraft dynamics, (p(L), f(L), g(L), h(L), k(L), t(L), m(L)), in Eqs. (6) and (7). In this procedure, the true longitude, L, replaces time, t, as the independent variable, therefore the dynamics in Eq. (1) must be transformed using the conversion factor

$$\frac{dt}{dL} = \left(\frac{dL}{dt}\right)^{-1},\tag{6}$$

so that the other states of the spacecraft, (p(L), f(L), g(L), h(L), k(L), m(L)), are given as

$$\frac{d}{dL}(p, f, g, h, k, L) = \frac{dt}{dL}\frac{d}{dt}(p, f, g, h, k, L).$$
(7)

The initial conditions are set as the LEO orbital elements in Table 2 that have been converted to modified equinoctial elements. The initial guess is integrated until the semi-parameter, p, of the orbit is equal to the corresponding terminal value, p_f . For the control, (T, u_r, u_t, u_n) , the thrust magnitude, T, is considered to be at maximum for the entirety of the integration and the thrust direction components are solved for afterwards by assuming that the thrust is always in the same direction as the velocity vector.

3.2 Initial Guess for Multiple Orbital Revolution Solutions

For the problem cases categorized as multiple orbital revolutions, an initial guess procedure was implemented [24]. The cases that contain multiple orbital revolutions require an initial guess that contains a number of orbital revolutions that is reasonably close to the actual number of orbital revolutions of the optimal solution. This initial guess procedure consists of solving a chain of optimal control sub-problems, where the goal is to minimize the following objective functional that consists of a mean square relative difference

$$J = \left[\frac{p(L_f) - p_D}{1 + p_D}\right]^2 + \left[\frac{f^2(L_f) + g^2(L_f) - e_D^2}{1 + e_D^2}\right]^2 + \left[\frac{h^2(L_f) + k^2(L_f) - \tan^2\left(\frac{i_D}{2}\right)}{\sec^2\left(\frac{i_D}{2}\right)}\right]^2, \quad (8)$$

by determining the state and control that transfers the spacecraft from the initial low-Earth orbit to the correct terminal orbit, depending on the study. When minimizing Eq. (8), the sub-problem attains an optimal solution that is as close in proximity as possible to the desired terminal semi-parameter, p_D , eccentricity, e_D , and inclination, i_D , within one orbital revolution. Each sub-problem uses the terminal state of the previous sub-problem as the initial state of the current sub-problem and is evaluated at most over one orbital revolution. It is noted that for the first sub-problem, the initial state is set as the LEO orbital elements in Table 2 that have been converted into modified equinoctial elements using Eq. (2). The procedure, then, is similar to that for the initial guess of Section 3.1 where the true longitude, L, replaces t as the independent variable and the dynamics are written in the form of Eq. (7).

The continuous-time optimal control sub-problem is then stated as follows. Minimize the objective functional in Eq. (8), subject to the dynamics constraints in Eqs. (6) and (7), the path constraint in Eq. (3), and the boundary conditions

$$p^{(n)}\left(L_{0}^{(n)}\right) \ = \ p^{(n-1)}\left(L_{f}^{(n-1)}\right), \qquad p^{(n)}\left(L_{f}^{(n)}\right) \ = \ \text{Free},$$

$$f^{(n)}\left(L_{0}^{(n)}\right) \ = \ f^{(n-1)}\left(L_{f}^{(n-1)}\right), \qquad f^{(n)}\left(L_{f}^{(n)}\right) \ = \ \text{Free},$$

$$g^{(n)}\left(L_{0}^{(n)}\right) \ = \ g^{(n-1)}\left(L_{f}^{(n-1)}\right), \qquad g^{(n)}\left(L_{f}^{(n)}\right) \ = \ \text{Free},$$

$$h^{(n)}\left(L_{0}^{(n)}\right) \ = \ h^{(n-1)}\left(L_{f}^{(n-1)}\right), \qquad h^{(n)}\left(L_{f}^{(n)}\right) \ = \ \text{Free},$$

$$k^{(n)}\left(L_{0}^{(n)}\right) \ = \ k^{(n-1)}\left(L_{f}^{(n-1)}\right), \qquad k^{(n)}\left(L_{f}^{(n)}\right) \ = \ \text{Free},$$

$$t^{(n)}\left(L_{0}^{(n)}\right) \ = \ t^{(n-1)}\left(L_{f}^{(n-1)}\right), \qquad t^{(n)}\left(L_{f}^{(n)}\right) \ = \ \text{Free},$$

$$m^{(n)}\left(L_{0}^{(n)}\right) \ = \ m^{(n-1)}\left(L_{f}^{(n-1)}\right), \qquad m^{(n)}\left(L_{f}^{(n)}\right) \ = \ \text{Free},$$

$$L_{0}^{(n)} \ = \ L_{f}^{(n-1)}, \qquad L_{f}^{(n)} \ \leq \ L_{f}^{(n-1)} + 2\pi,$$

for $n = 1, \dots, N$, where N is the total number of true longitude cycles. The sub-problem solutions are combined into an initial guess once the desired terminal conditions of the terminal orbital

elements in Table 2 are within an error tolerance of 10^{-4} .

The sub-problems are solved using the general-purpose MATLAB optimal control software $\mathbb{GPOPS} - \mathbb{II}$ [21] together with the nonlinear program (NLP) solver IPOPT [25] in full Newton (second derivative) mode with an NLP solver tolerance of 10^{-7} . All derivatives required by IPOPT were obtained using the open-source algorithmic differentiation software ADiGator [26]. $\mathbb{GPOPS} - \mathbb{II}$ was employed using the following settings. First, an initial guess is created using the ordinary differential equations solver odel13, where the ODE solver integrates the spacecraft dynamics, (p(L), f(L), g(L), h(L), k(L), t(L), m(L)), in Eqs. [6] and [7]. The initial conditions are set as the LEO orbital elements in Table [2] that have been converted to modified equinoctial elements using Eq. [2] for the first sub-problem and then, for every subsequent sub-problem, the initial conditions are set as the terminal values of the previous sub-problem. The initial guess is integrated for one orbital revolution, where the thrust magnitude, T, is considered to be at maximum for the entirety of the integration and the thrust direction components, (u_r, u_t, u_n) , are solved for afterwards by assuming that the thrust is always in the same direction as the velocity vector. Second, a hp-adaptive mesh refinement method [27] is used with a mesh refinement accuracy tolerance of 10^{-2} . Third, the initial mesh is set to have one mesh interval with four collocation points.

4 Numerical Approach: BBSOC Method

Numerical solutions to the minimum-fuel orbital transfer problems described in Section 2 are obtained using the recently developed bang-bang and singular optimal control (BBSOC) method developed in Ref. 20. The BBSOC method implements a multiple-domain formulation of Legendre-Gauss-Radau (LGR) collocation 28–32 together with an algorithm developed specifically for detecting and solving bang-bang and singular optimal control problems. In particular, the BBSOC method identifies the existence of switches in the optimal control, where these switches may either be bang arcs (that is, segments where the control lies at one of its limits) or singular arcs (that

is, segments where the Pontryagin's minimum principle fails to yield a complete solution to the optimal control problem). For segments identified as singular arcs, the BBSOC method performs an iterative regularization procedure to compute the singular control. For segments identified as bang-bang, the BBSOC method determines whether the control lies at either its lower or upper limit and optimize values of the switch times. Once the switching structure is identified using the Hamiltonian, the BBSOC method partitions the initial mesh into one or more domains, where each domain is used to determine the control in that particular part of the solution. As part of the domain partitioning, the times at which the switches occur are introduced as variables in the optimization and are determined as part of the solution process. Figure 1 shows how the BBSOC method obtains an optimized nonsmooth control structure.

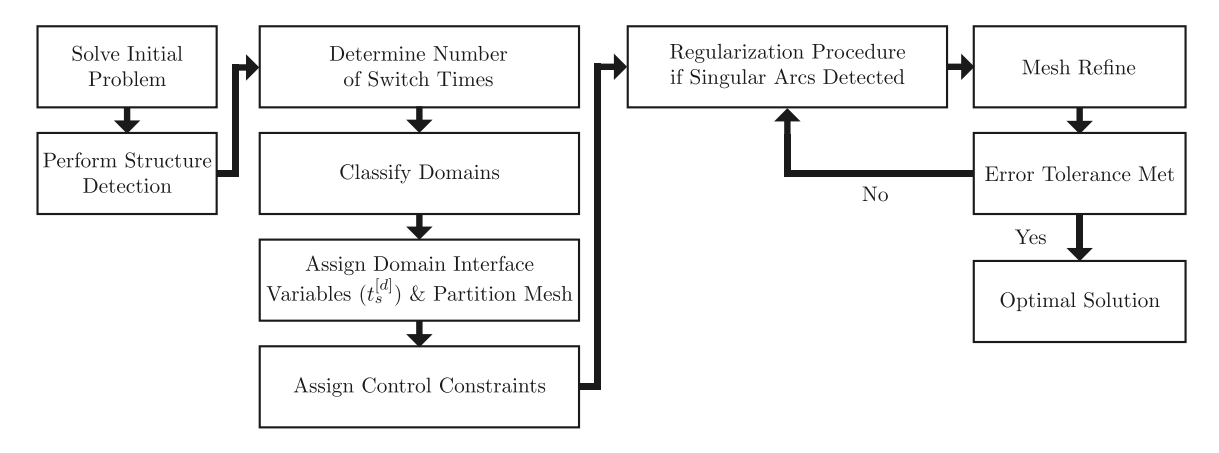


Figure 1: Description of the BBSOC method.

Unlike previous studies in the literature where singular arcs are assumed to not exist in the orbital transfer problem, in this research singular arcs are considered. It is noted, however, that for the results obtained in this paper the BBSOC method never detected the existence of a singular arc in the optimal solution and only detected a bang-bang structure in the control. As a result, in this paper the BBSOC method determines the optimal bang-bang switching structure in the optimal control without a priori knowledge of this structure. More details on the BBSOC method and the multiple-domain LGR collocation can be found in Ref. [20].

5 Results and Discussion

Each of the three orbital transfer studies is solved in canonical units (that is, where the gravitational parameter is unity) with the value of maximum allowable thrust acceleration, s_0 shown in Table 4. All results were obtained using BBSOC method of Ref. 20 implemented in MATLAB® with the NLP problem solver IPOPT 25 employed in full Newton (second derivative) mode with an NLP solver tolerance of 10^{-7} and the mesh refinement method described in Ref. 32. All derivatives required by IPOPT are computed using the algorithmic differentiation software ADiGator 26. All computations were performed using a 2.9 GHz 6-Core Intel Core i9 MacBook Pro running Mac OS version 11.6.1 (Big Sur) with 32GB 2400MHz DDR4 RAM and MATLAB® Version R2018b (build 9.5.0.944444).

5.1 Overall Performance of Optimized Orbital Transfers

Tables 5-7 show the overall performance for the LEO-to-MEO, LEO-to-HEO, and LEO-to-GEO transfers, respectively. In particular, Tables 5-7 show the terminal mass, $m(t_f)$, the total thrusting time, t_T , the total number of revolutions, N, the number of thrust arcs, A_T , and the total impulse, ΔV , for the seven values of maximum allowable thrust acceleration, s_0 , studied. In addition, for those values of s_0 that appear in Ref. 4, the impulse, 4-4, obtained in Ref. 4-4 is shown in Tables 5-7. When computing the impulse, 4-4, the Tsiolkovsky rocket equation

$$\Delta V = g_0 I_{sp} \ln \left[\frac{m_0}{m(t_f)} \right]. \tag{10}$$

is used. For all three types of transfers the solutions can be separated into two categories: orbital transfers with partial orbital revolutions and orbital transfers with multiple orbital revolutions. In particular, regardless of the type of transfer, the partial revolution transfers correspond to larger values of s_0 (Cases 1-4), whereas the multiple revolution transfers correspond to smaller values of s_0 (Cases 5-7). Furthermore, as s_0 decreases, the terminal mass decreases, the total time thrusting increases, the total number of orbital revolutions increases, and the total impulse increases. It is

noted that, for the partial orbital revolution solutions, each case has two thrust arcs whereas, for the multiple orbital revolution solutions, the number of thrust arcs increases as s_0 decreases. It is noted that the terminal mass decreases as s_0 decreases because the total time thrusting increases which leads to an increase in fuel consumption in order to attain the required terminal conditions. When comparing the total impulse of this work to the total impulse obtained in Ref. [4] (that is, for the four overlapping cases of maximum allowable thrust acceleration), it can be seen that this work produces a smaller ΔV (except for Case 1 of Study 2). For Cases 1 and 3, the differences in ΔV are relatively small because the solutions for these cases consist of only two thrust arcs (that is, burn-coast-burn) which is similar to the burn-coast-burn thrusting structure assumed in Ref. 4. Note, however, that for Cases 1 and 3 the burn-coast-burn thrusting structure is obtained algorithmically via the BBSOC method without any a priori assumptions. On the other hand, for Cases 5 and 7 the differences in ΔV are significantly larger because the optimal control consists of significantly more than two thrust arcs which thereby shows that the burn-coast-burn thrusting structure assumed in Ref. 4 is less fuel efficient. Therefore, the ΔV obtained in this research is similar to the ΔV obtained in Ref. 4 when the BBSOC method produces a thrusting structure similar to the assumed thrusting structure in Ref. $\boxed{4}$ and produces a significantly lower ΔV as the BBSOC method produces a thrusting structure that significantly differs from the assumed thrusting structure of Ref. [4].

Aside: It is noted for the LEO-to-HEO transfers that Cases 1 and 2 require that a procedure different from that described in Section 3 because the procedure used in Section 3 using the initial setup $(\eta, M, c_p) = (0.01, 20, 3)$ did not detect the bang-bang structure of the optimal control. In order to detect the bang-bang structure for these cases, via some experimentation the following alternate procedure was used. First, a second initial setup $(\eta, M, c_p) = (0.1, 10, 3)$ was used. The solution obtained using this second setup is then used as an initial guess with yet a third initial setup $(\eta, M, c_p) = (0.001, 70, 3)$. The results obtained using this alternate procedure led to the

results shown in Table 6. The solution for Case 2 shown in Table 6 is then used as an initial guess for Case 1 using the initial setup $(\eta, M, c_p) = (0.1, 10, 3)$. The solution obtained using this last setup is then used as an initial guess with the setup $(\eta, M, c_p) = (0.01, 170, 3)$, leading to the results found in Table 6.

Table 5: Performance results for Study 1: LEO-to-MEO transfers.

Case	$s_0 \left(\mathbf{m} \cdot \mathbf{s}^{-2} \right)$	$m\left(t_{f}\right)\;\left(\mathrm{kg}\right)$	t_T (h)	N	A_T	$\Delta V \ \left(\mathbf{m} \cdot \mathbf{s}^{-1} \right)$	Ref. $4 \Delta V \text{ (m} \cdot \text{s}^{-1})$
1	10	674.9651	0.0880	0.5196	2	3854.9	3863
2	5	674.7867	0.1744	0.5352	2	3857.5	_
3	1	668.2949	0.8941	0.7398	2	3952.3	3970
4	0.5	653.0154	1.8816	0.8768	2	4179.1	_
5	0.1	624.2352	10.2132	4.9579	4	4621.2	4731
6	0.05	607.2275	21.2975	9.1414	6	4892.1	_
7	0.01	606.9697	106.4970	32.8742	9	4896.2	5122

Table 6: Performance results for Study 2: LEO-to-HEO transfers.

Case	$s_0 \ \left(\mathbf{m} \cdot \mathbf{s}^{-2} \right)$	$m\left(t_{f}\right)\;\left(\mathrm{kg}\right)$	t_T (h)	N	A_T	$\Delta V \ \left(\mathbf{m} \cdot \mathbf{s}^{-1} \right)$	Ref. 4 $\Delta V \ (\text{m} \cdot \text{s}^{-1})$
1	10	716.2925	0.0766	0.5202	2	3272.2	3271
2	5	715.7138	0.1525	0.5387	2	3280.1	_
3	1	699.2824	0.8140	0.8359	2	3507.8	3555
4	0.5	663.1665	1.8242	0.9240	2	4027.9	_
5	0.1	657.2695	9.2494	4.9570	6	4115.6	5271
6	0.05	645.0881	19.1564	9.0376	9	4298.9	_
7	0.01	576.7825	114.7384	39.0413	17	5396.5	6109

Table 7: Performance results for Study 3: LEO-to-GEO transfers.

Case	$s_0 \left(\mathbf{m} \cdot \mathbf{s}^{-2} \right)$	$m\left(t_f\right) \; (\mathrm{kg})$	t_T (h)	N	A_T	$\Delta V \ \left(\mathbf{m} \cdot \mathbf{s}^{-1} \right)$	Ref. 4 $\Delta V \ (\text{m} \cdot \text{s}^{-1})$
1	10	656.7935	0.0925	0.5195	2	4122.6	4127
2	5	656.3850	0.1857	0.5408	2	4128.7	_
3	1	646.4416	0.9614	0.7694	2	4278.4	4308
4	0.5	626.2787	2.0140	0.9380	2	4589.1	_
5	0.1	619.0090	10.3158	4.8044	5	4703.6	5167
6	0.05	583.7997	22.5498	8.0286	6	5277.9	_
7	0.01	579.8979	114.0104	110.0091	8	5343.7	5698

5.2 Key Features of Optimized Solutions

In this section the key features of the optimized LEO-to-MEO, LEO-to-HEO, and LEO-to-GEO transfers is analyzed by studying the solution for Case 5, $s_0 = 0.1 \text{ m} \cdot \text{s}^{-2}$. Each type of transfer is studied separately in order to highlight the key features of the solution for that type of transfer.

5.2.1 Key Features of Optimized LEO-to-MEO Transfers

Figure 2 shows the optimized three-dimensional trajectory of the LEO-to-MEO transfer, where the modified equinoctial elements were converted into scaled Cartesian coordinates 22. It is seen that the spacecraft begins in a low-Earth orbit and terminates in a medium-Earth orbit that corresponds to the orbital elements in Table 2. The optimal trajectory of the spacecraft consists of 4.9579 orbital revolutions around the Earth with a final mass of 624.2352 kg, four thrust arcs, a total time thrusting of 10.2132 h, and a total impulse of 4621.2 m·s⁻¹. It is noted that all of the thrust arcs, except for the final, occur near the periapsis of the orbit.

Figure 3 shows the behavior of the orbital elements of the optimized trajectory of the spacecraft. The semi-major axis, a, increases throughout all of the thrust arcs from 7.003×10^6 m to 2.6560×10^7 m, where the change becomes more rapid in the later thrust arcs. It is more fuel efficient to

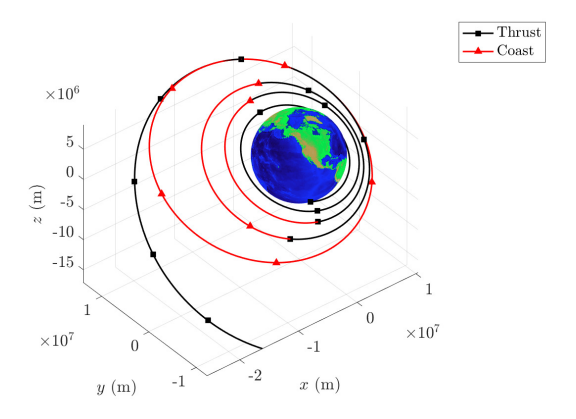


Figure 2: Optimal three-dimensional spacecraft trajectory for LEO-to-MEO transfer with $s_0 = 0.1 \text{ m} \cdot \text{s}^{-2}$.

change the size of the orbit near periapsis because the velocity of the spacecraft is the fastest the spacecraft will travel on that specific orbit, meaning that the amount of fuel expended is less to achieve a higher velocity in the same direction than anywhere else on the orbit. Therefore, the thrust arcs happen near periapsis. The eccentricity, e, increases through the first three thrust arcs from 0 to 0.3579, then decreases to zero during the last thrust arc. The eccentricity rapidly changes during the first three thrust arcs because it is more fuel efficient to increase the size of the orbit first and get further from the Earth, then followed by changing the inclination of the orbit. The last thrust arc then places the spacecraft into the final circular orbit. The inclination, i, increases slowly from 28.5 deg to 32.8764 deg during the first three thrust arcs, and then rapidly increases to 54.7 deg during the final thrust arc. The inclination changes by 4.3764 deg during the first three thrust arcs and by 21.8236 deg during the final thrust arc. The inclination changes much more significantly during the final thrust arc than in the first three thrust arcs because the spacecraft is farther away from the Earth, therefore the velocity of the spacecraft is smaller. Consequently, the maneuver is more fuel efficient because inclination changes require a change in the direction of velocity. Therefore, when the velocity is smaller the maneuver will require less fuel to be expended, so the inclination changes more during the final thrust arc.

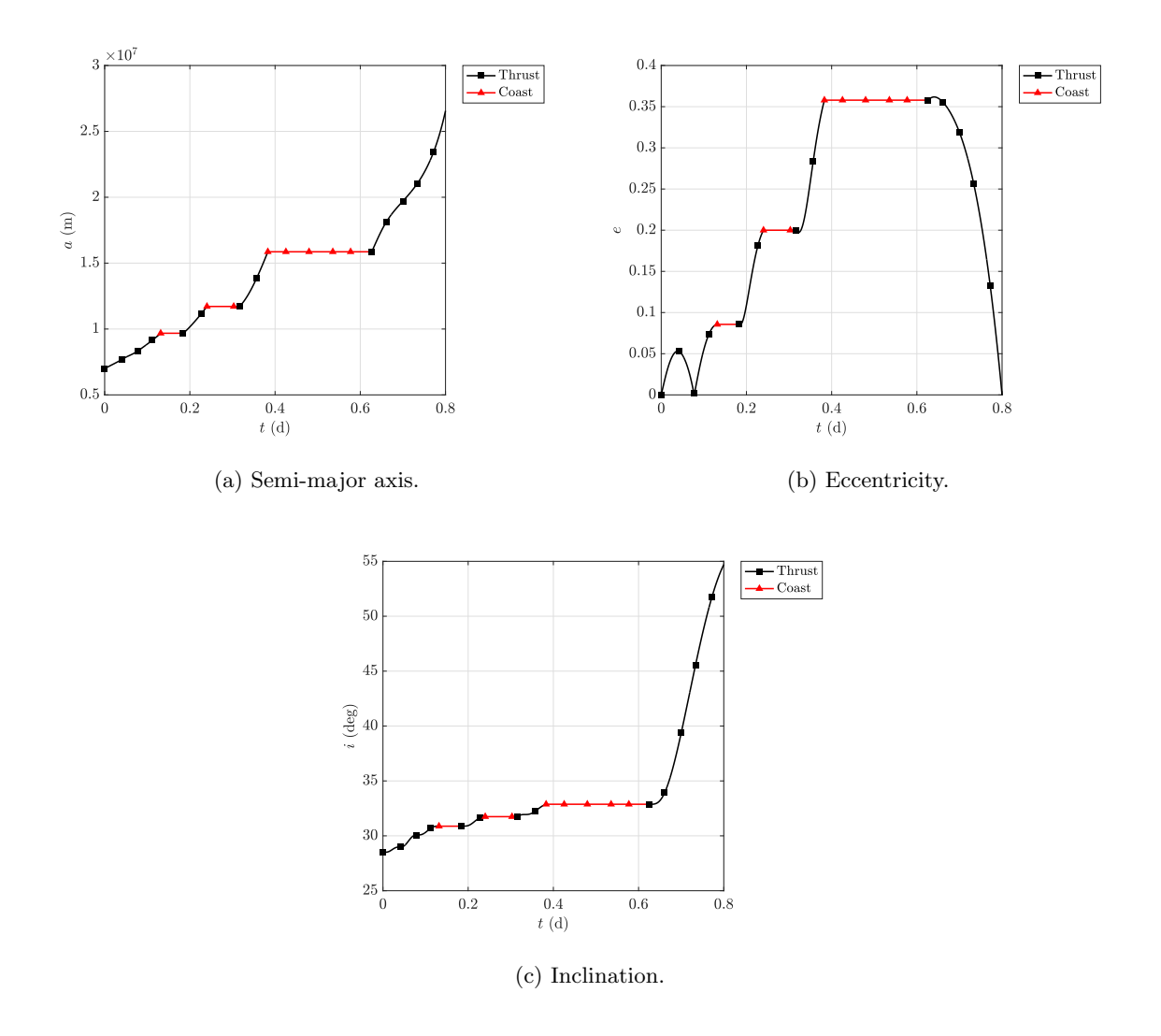


Figure 3: Orbital elements along optimal trajectory for LEO-to-MEO transfer with $s_0 = 0.1 \text{ m} \cdot \text{s}^{-2}$.

Figure 4 shows the mass of the spacecraft throughout the fuel-optimized trajectory. The mass decreases steadily throughout the four thrust arcs from 1000 kg to 624.2352 kg, which is the optimized final mass. For Case 5 of the LEO-to-MEO transfer, the amount of fuel expended is 375.7648 kg.

Finally, Fig. 5 shows the control components of the optimal trajectory, which are the thrust magnitude, T, and the thrust direction components, (u_r, u_t, u_n) . The thrust magnitude remains at the maximum thrust $T_{\text{max}} = 100 \text{ N}$ for the duration of the thrust arcs and 0 N for the duration of the coast arcs. There are four thrust arcs and three coast arcs in the optimized thrusting structure. Consequently, the thrust has six discontinuities and the structure of this solution is bang-bang.

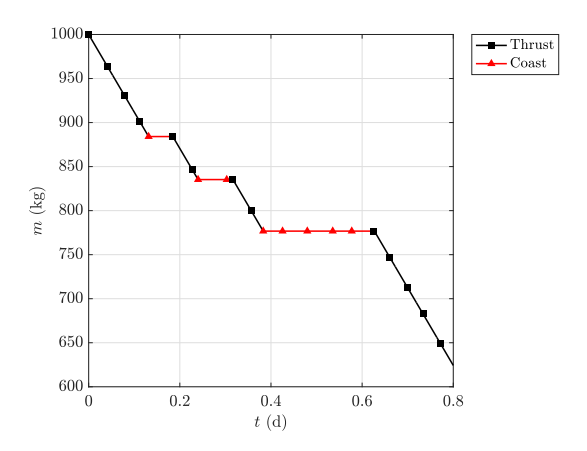


Figure 4: Mass of spacecraft along optimal trajectory for LEO-to-MEO transfer with $s_0 = 0.1 \text{ m} \cdot \text{s}^{-2}$.

It is noted that the structure of the thrust is not assumed before solving the problem and the structure is detected using the BBSOC method [20]. The components of the thrust direction are only applicable when the thrust is non-zero (that is, the four thrust arcs), therefore the behavior will only be discussed for the thrust arcs because the components are set to zero during the coast arcs on the plot for clarity. The radial thrust direction component, u_r , increases from -0.1435 to 0.3569 throughout the first three thrust arcs, where the direction oscillates about 0 with increasing amplitudes, then decreases from 0.4665 to 0.1319 during the final thrust arc. The transverse thrust direction component, u_t , decreases from 0.9682 to 0.9004 throughout the first three thrust arcs, then decreases from 0.8842 to 0.7693 in the final thrust arc. The normal thrust direction component, u_n , increases from -0.2048 to 0.2488 throughout the first three thrust arcs, where the direction oscillates, then decreases from 0.0242 to -0.6251 during the final thrust arc. This behavior demonstrates that during the first three thrust arcs the majority of the thrust is in the transverse direction in order to increase the size of the orbit from 7.003×10^6 m to 1.5862×10^7 m and that during the final thrust arc the majority of the thrust is in the transverse and normal directions to increase the size of the orbit from 1.5862×10^7 m to 2.6560×10^7 m and increase the inclination of the orbit from 32.8764 deg to 54.7 deg.

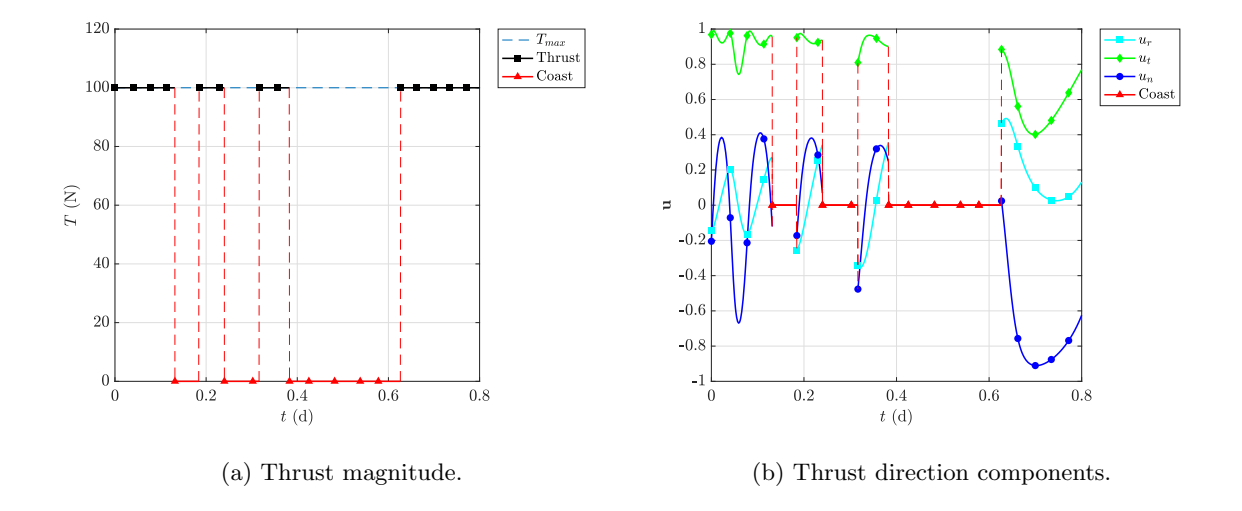


Figure 5: Optimal control for LEO-to-MEO transfer with $s_0 = 0.1 \text{ m} \cdot \text{s}^{-2}$.

5.2.2 Key Features of Optimized LEO-to-HEO Transfers

Figure 6 shows the optimized three-dimensional trajectory of the LEO-to-HEO transfer, where the modified equinoctial elements were converted into scaled Cartesian coordinates 22. It is seen that the spacecraft begins in a low-Earth orbit and terminates in a high-Earth orbit that corresponds to the orbital elements in Table 2. The optimal trajectory of the spacecraft consists of 4.9570 orbital revolutions around the Earth with a final mass of 657.2695 kg, six thrust arcs, a total time thrusting of 9.2494 h, and a total impulse of 4115.6 m·s⁻¹. It is noted that all of the thrust arcs, except for the final thrust arc, occur near periapsis of the transfer orbit.

Figure 7 shows the behavior of the orbital elements of the optimized trajectory of the spacecraft. The semi-major axis, a, increases throughout the first five thrust arcs from 7.003×10^6 m to 2.8177×10^7 m, and then decreases to 2.6578×10^7 m during the final thrust arc. It is more fuel efficient to change the size of the orbit near periapsis because the velocity of the spacecraft is the fastest the spacecraft will travel on that specific orbit, meaning that the amount of fuel expended is less to achieve a higher velocity in the same direction than anywhere else on the orbit. Therefore, the size of the orbit is changed the most during the fifth thrust arc. The eccentricity, e, increases throughout all of the thrust arcs from 0 to 0.73646. The eccentricity rapidly changes during the

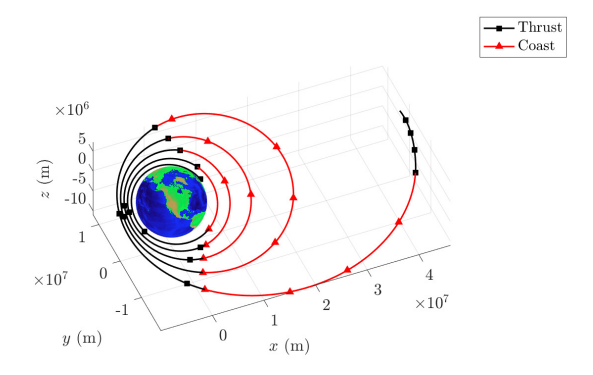


Figure 6: Optimal three-dimensional spacecraft trajectory for LEO-to-HEO transfer with $s_0 = 0.1 \text{ m} \cdot \text{s}^{-2}$.

first five thrust arcs because it is more fuel efficient to change the size of the orbit first and get far from the Earth, then followed by changing the inclination of the orbit. The inclination, i, slowly increases from 28.5 deg to 29.8969 deg during the first five thrust arcs, and then rapidly increases to 63.435 deg during the final thrust arc. The inclination changes by 1.3969 deg during the first five thrust arcs and by 33.5381 deg during the final thrust arc. The inclination changes much more significantly during the final thrust arc than in the first five thrust arcs because the spacecraft is farther away from the Earth, therefore the velocity of the spacecraft is smaller. Consequently, the maneuver is more fuel efficient because inclination changes require a change in the direction of velocity. Therefore, when the velocity is smaller the maneuver will require less fuel to be expended, so the inclination changes more during the final thrust arc.

Figure 8 shows the mass of the spacecraft throughout the fuel-optimized trajectory. The mass decreases steadily throughout the six thrust arcs from 1000 kg to 657.2695 kg, which is the optimized final mass. For Case 5 of the LEO-to-HEO transfer, the amount of fuel expended is 342.7305 kg.

Finally, Fig. 9 shows the control components of the optimal trajectory, which are the thrust magnitude, T, and the thrust direction components, (u_r, u_t, u_n) . The thrust magnitude remains at the maximum thrust $T_{\text{max}} = 100 \text{ N}$ for the duration of the thrust arcs and 0 N for the duration of

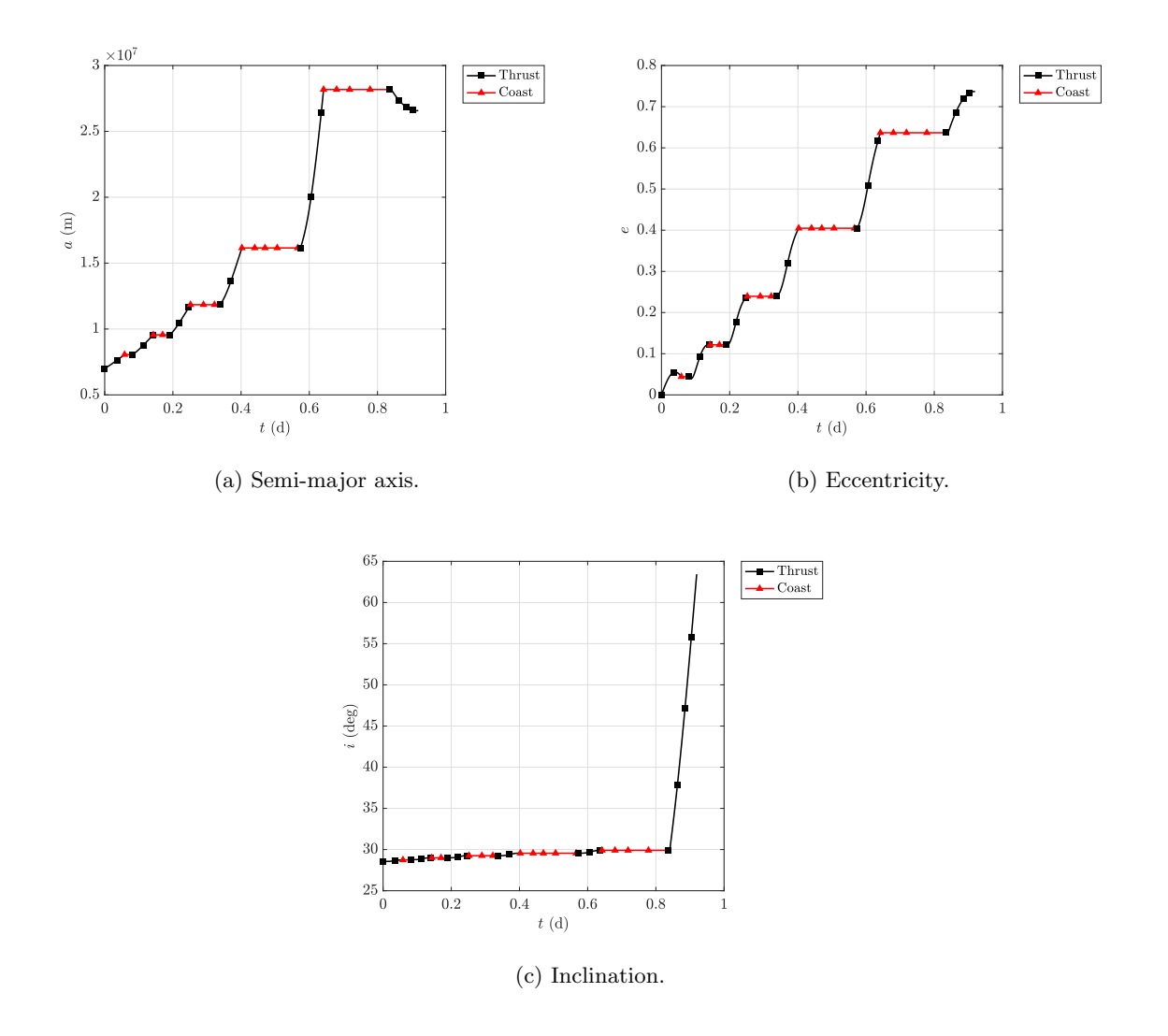


Figure 7: Orbital elements along optimal trajectory for LEO-to-HEO transfer with $s_0 = 0.1 \text{ m} \cdot \text{s}^{-2}$.

the coast arcs. There are six thrust arcs and five coast arcs in the optimized thrusting structure. Consequently, the thrust has ten discontinuities and the structure of this solution is bang-bang. It is noted that the structure of the thrust is not assumed before solving the problem and the structure is detected using the BBSOC method [20]. The components of the thrust direction are only applicable when the thrust is non-zero (that is, the six thrust arcs), therefore the behavior will only be discussed for the thrust arcs because the components are set to 0 during the coast arcs on the plot for clarity. The radial thrust direction component, u_r , increases from -0.1074 to 0.6782 throughout the first five thrust arcs, where the direction oscillates about 0 with increasing amplitudes, then decreases from 0.0920 to -0.0157 during the final thrust arc. The transverse

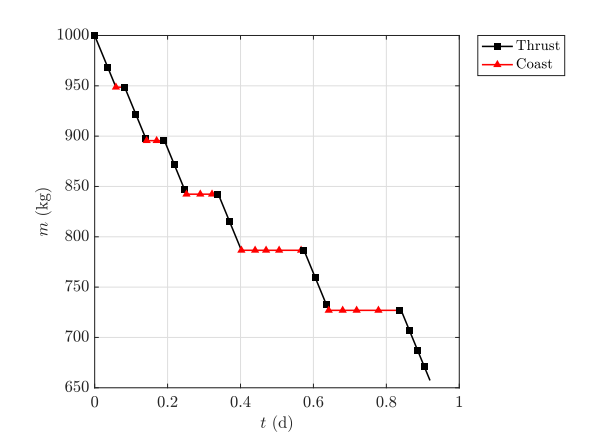


Figure 8: Mass of spacecraft along optimal trajectory for LEO-to-HEO transfer with $s_0 = 0.1 \text{ m} \cdot \text{s}^{-2}$.

thrust direction component, u_t , decreases from 0.9712 to 0.7348 throughout the first five thrust arcs, where the direction changes in an inverted parabolic pattern during the thrust arcs, then increases from -0.5176 to 0.0346 in the final thrust arc. The normal thrust direction component, u_n , decreases from 0.2125 to -0.0062 throughout the first five thrust arcs, where the direction changes in a parabolic pattern during the thrust arcs, then increases from 0.8506 to 0.9997 during the final thrust arc. This behavior demonstrates that during the first five thrust arcs the majority of the thrust is in the transverse direction in order to increase the size of the orbit from 7.003×10^6 m to 2.8177×10^7 m and that during the final thrust arc the majority of the thrust is in the normal direction to increase the inclination of the orbit from 29.8969 deg to 63.435 deg.

5.2.3 Key Features of Optimized LEO-to-GEO Transfers

Figure $\boxed{10}$ shows the optimized three-dimensional trajectory of the LEO-to-GEO transfer, where the modified equinoctial elements were converted into scaled Cartesian coordinates $\boxed{22}$. It is seen that the spacecraft begins in a low-Earth orbit and terminates in a geostationary orbit that corresponds to the orbital elements in Table $\boxed{2}$. The optimal trajectory of the spacecraft consists of 4.8044 orbital revolutions around the Earth with a final mass of 619.0090 kg, five thrust arcs, a total time thrusting of 10.3158 h, and a total impulse of 4703.6 m·s⁻¹. It is noted that all of the thrust arcs,

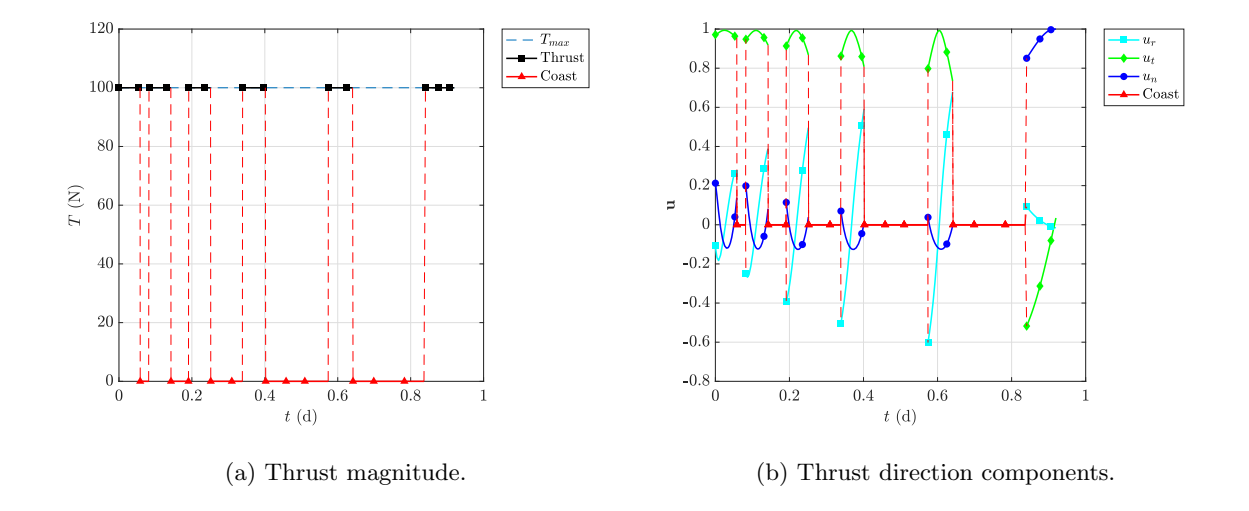


Figure 9: Optimal control for LEO-to-HEO transfer with $s_0 = 0.1 \text{ m} \cdot \text{s}^{-2}$.

except for the final, occur near the periapsis of the orbit.

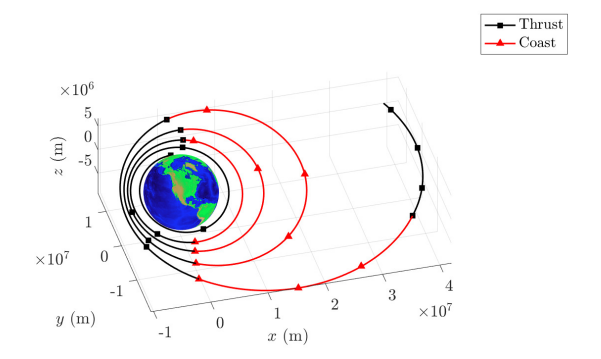


Figure 10: Optimal three-dimensional spacecraft trajectory for LEO-to-GEO transfer with $s_0 = 0.1 \text{ m} \cdot \text{s}^{-2}$.

Figure 11 shows the behavior of the orbital elements of the optimized trajectory of the spacecraft. The semi-major axis, a, increases throughout all of the thrust arcs from 7.003×10^6 m to 4.2287×10^7 m, where the change becomes more rapid in the later thrust arcs. It is more fuel efficient to change the size of the orbit near periapsis because the velocity of the spacecraft is the fastest the spacecraft will travel on that specific orbit, meaning that the amount of fuel expended is less to achieve a higher velocity in the same direction than anywhere else on the orbit. Therefore, the

thrust arcs happen near periapsis, except for the final thrust arc. The eccentricity, e, increases through the first four thrust arcs from 0 to 0.5874, then decreases to 0 during the last thrust arc. The eccentricity rapidly changes during the first four thrust arcs because it is more fuel efficient to increase the size of the orbit first and get far from the Earth, then followed by changing the inclination of the orbit. The last thrust arc then creates a circular orbit. The inclination, i, slowly decreases from 28.5 deg to 25.8893 deg during the first four thrust arcs, and then rapidly decreases to 0 deg during the final thrust arc. The inclination changes by 2.6107 deg during the first four thrust arcs and by 25.8893 deg during the final thrust arc. The inclination changes much more significantly during the final thrust arc than in the first four thrust arcs because the spacecraft is farther away from the Earth, therefore the velocity of the spacecraft is smaller. Consequently, the maneuver is more fuel efficient because inclination changes require a change in the direction of velocity. Therefore, when the velocity is smaller the maneuver will require less fuel to be expended, so the inclination changes more during the final thrust arc.

Figure 12 shows the mass of the spacecraft throughout the fuel-optimized trajectory. The mass decreases steadily throughout the five thrust arcs from 1000 kg to 619.0090 kg, which is the optimized final mass. For Case 5 of the LEO-to-GEO transfer, the amount of fuel expended is 380.9910 kg.

Finally, Fig. [13] shows the control components of the optimal trajectory, which are the thrust magnitude, T, and the thrust direction components, (u_r, u_t, u_n) . The thrust magnitude remains at the maximum thrust $T_{\text{max}} = 100 \text{ N}$ for the duration of the thrust arcs and 0 N for the duration of the coast arcs. There are five thrust arcs and four coast arcs in the optimized thrusting structure. Consequently, the thrust has eight discontinuities and the structure of this solution is bang-bang. It is noted that the structure of the thrust is not assumed before solving the problem and the structure is detected using the BBSOC method [20]. The components of the thrust direction are only applicable when the thrust is non-zero (that is, the five thrust arcs), therefore the behavior

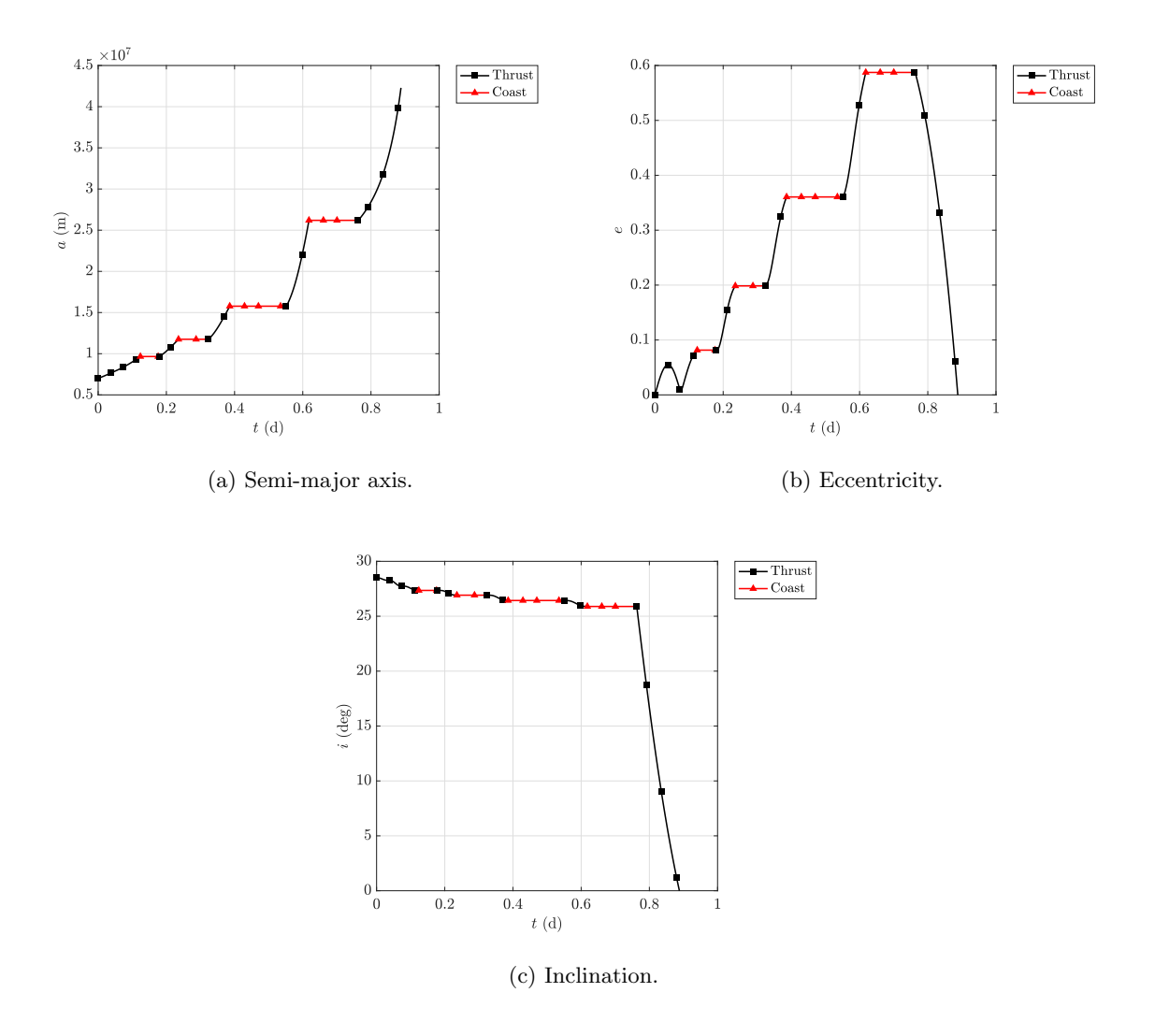


Figure 11: Orbital elements along optimal trajectory for LEO-to-GEO transfer with $s_0 = 0.1 \text{ m} \cdot \text{s}^{-2}$.

will only be discussed for the thrust arcs because the components are set to 0 during the coast arcs on the plot for clarity. The radial thrust direction component, u_r , increases from -0.1167 to 0.4551 throughout the first four thrust arcs, where the direction oscillates about 0 with increasing amplitudes, then decreases from 0.1253 to 0.0929 during the final thrust arc. The transverse thrust direction component, u_t , decreases from 0.9932 to 0.8900 throughout the first four thrust arcs, then increases from 0.5368 to 0.8313 in the final thrust arc. The normal thrust direction component, u_n , increases from 0.0051 to 0.0288 throughout the first three thrust arcs, where the direction oscillates, then increases from -0.8343 to -0.5481 during the final thrust arc. This behavior demonstrates that during the first four thrust arcs the majority of the thrust is in the transverse direction in

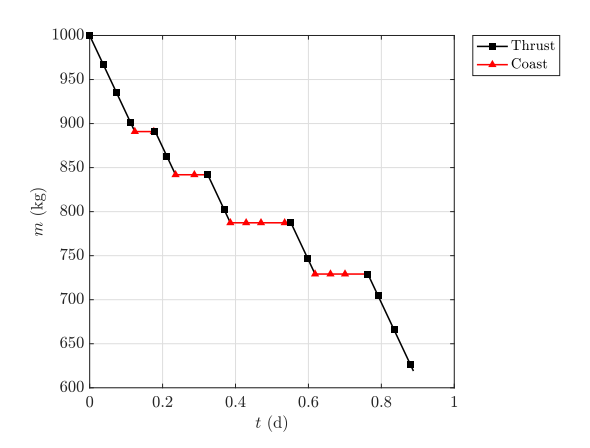


Figure 12: Mass of spacecraft along optimal trajectory for LEO-to-GEO transfer with $s_0=0.1~{\rm m\cdot s^{-2}}$.

order to increase the size of the orbit from 7.003×10^6 m to 2.6198×10^7 m and that during the final thrust arc the majority of the thrust is in the transverse and normal directions to increase the size of the orbit from 2.6198×10^7 m to 4.2287×10^7 m and decrease the inclination of the orbit from 25.8893 deg to 0 deg.

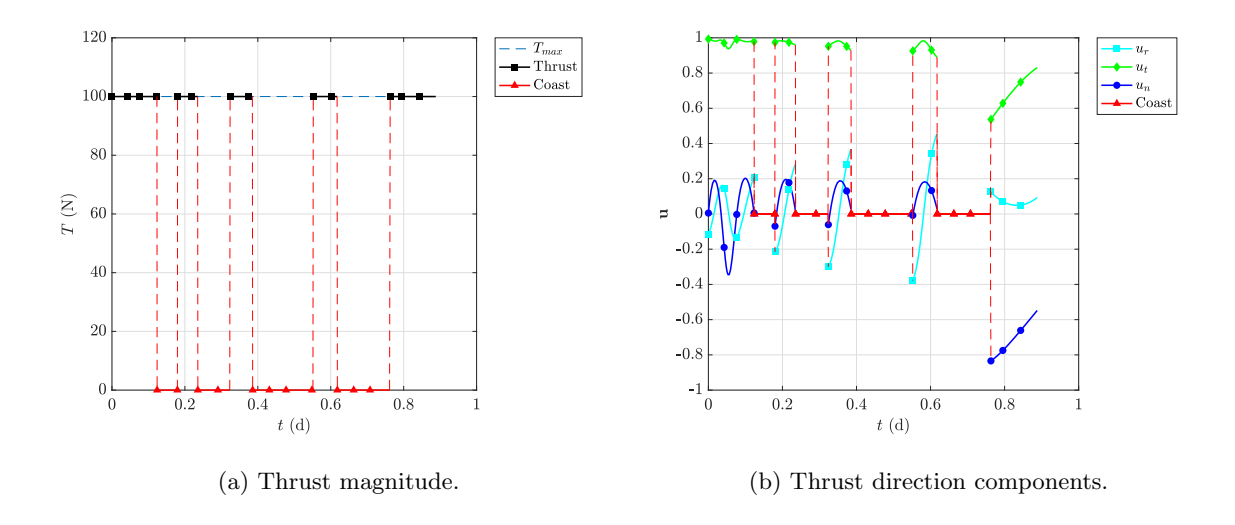


Figure 13: Optimal control for LEO-to-GEO transfer with $s_0 = 0.1 \text{ m} \cdot \text{s}^{-2}$.

6 Conclusions

A numerical optimization study of various minimum-fuel Earth-based orbital transfers from low-Earth orbit (LEO) to both medium-Earth orbit (MEO) and high-Earth orbit (HEO) was performed. The optimal orbital transfer trajectory optimization problem has been formulated as a nonlinear optimal control problem. The problem was solved using a multiple-domain formulation of Legendre-Gauss-Radau (LGR) collocation together with a method called the bang-bang and singular optimal control (BBSOC) method. The BBSOC method partitions the domain of the independent variable based on identifying segments where the control is either at one of its limits (bang-bang) or is singular. A key feature of the results obtained in this research is that the optimal switching structure of the thrust was not assumed a priori but was determined using the BBSOC method. It was found for cases where the thrust switched many times during the maneuver that the minimum impulse obtained in this study was significantly lower than that obtained in a previous study where the thrust was allowed to switch only once during the maneuver. As an expected outcome, the results of this study show that improvement in fuel consumption is obtained when it is possible to determine the switching structure in the control as opposed to assuming a particular switching structure in the control a priori.

Acknowledgments

The authors gratefully acknowledge support for this research from the U.S. National Science Foundation under grant CMMI-2031213 and the National Aeronautics and Space Administration under grant NNX15AI10H through the University of Central Florida NASA Space Grant Consortium and Space Florida.

References

[1] Scheel, W. A. and Conway, B. A., "Optimization of very-low-thrust, many-revolution space-craft trajectories," *Journal of Guidance, Control, and Dynamics*, Vol. 17, No. 6, 1994, pp. 1185–1192. https://doi.org/10.2514/3.21331.

- [2] Betts, J. T., "Very low-thrust trajectory optimization using a direct SQP method," Journal of Computational and Applied Mathematics, Vol. 120, No. 1-2, 2000, pp. 27-40. https://doi.org/10.1016/S0377--0427(00)00301--0.
- [3] Kluever, C. A. and Oleson, S. R., "Direct Approach for Computing Near-Optimal Low-Thrust Earth-Orbit Transfers," *Journal of Spacecraft and Rockets*, Vol. 35, No. 4, 1998, pp. 509–515. https://doi.org/10.2514/2.3360.
- [4] Herman, A. L. and Spencer, D. B., "Optimal, Low-Thrust Earth-Orbit Transfers Using Higher-Order Collocation Methods," *Journal of Guidance, Control, and Dynamics*, Vol. 25, No. 1, 2002, pp. 40–47. https://doi.org/10.2514/2.4873.
- [5] Yang, G., "Direct Optimization of Low-thrust Many-revolution Earth-orbit Transfers," Chinese Journal of Aeronautics, Vol. 22, No. 4, 2009, pp. 426-433. https://doi.org/10.1016/S1000--9361(08)60121--1.
- [6] Gao, Y. and Li, X., "Optimization of low-thrust many-revolution transfers and Lyapunov-based guidance," Acta Astronautica, Vol. 66, No. 1-2, 2010, pp. 117-129. https://doi.org/10.1016/j.actaastro.2009.05.013.
- [7] Graham, K. F. and Rao, A. V., "Minimum-Time Trajectory Optimization of Many Revolution Low-Thrust Earth-Orbit Transfers," *Journal of Spacecraft and Rockets*, Vol. 52, No. 3, May–June 2015, pp. 711–727. https:doi.org/10.2514/1.A33187.
- [8] Rauwolf, G. A. and Coverstone-Carroll, V. L., "Near-optimal low-thrust orbit transfers generated by a genetic algorithm," *Journal of Spacecraft and Rockets*, Vol. 33, No. 6, 1996, pp. 859–862. https://doi.org/10.2514/3.26850.
- [9] Dachwald, B., "Optimization of very-low-thrust trajectories using evolutionary neurocontrol," Acta Astronautica, Vol. 57, No. 2-8, 2005, pp. 175-185. https://doi.org/10.1016/j.actaastro.2005.03.004.
- [10] Gergaud, J. and Haberkorn, T., "Homotopy method for minimum consumption orbit transfer problem," *ESAIM: Control, Optimisation and Calculus of Variations*, Vol. 12, No. 2, 2006, pp. 294–310. https://doi.org/10.1051/cocv:2006003.
- [11] Guo, T., Jiang, F., and Li, J., "Homotopic approach and pseudospectral method applied jointly to low thrust trajectory optimization," *Acta Astronautica*, Vol. 71, 2012, pp. 38–50. https://doi.org/10.1016/j.actaastro.2011.08.008.
- [12] Jiang, F., Baoyin, H., and Li, J., "Practical Techniques for Low-Thrust Trajectory Optimization with Homotopic Approach," *Journal of Guidance, Control, and Dynamics*, Vol. 35, No. 1, 2012, pp. 245–258. https://doi.org/10.2514/1.52476.
- [13] Coverstone-Carroll, V., Hartmann, J. W., and Mason, W. J., "Optimal multi-objective low-thrust spacecraft trajectories," Computer Methods in Applied Mechanics and Engineering, Vol. 186, No. 2–4, 2000, pp. 387–402. https://doi.org/10.1016/S0045--7825(99) 00393--X.
- [14] Zuiani, F., Vasile, M., Palmas, A., and Avanzini, G., "Direct transcription of low-thrust trajectories with finite trajectory elements," *Acta Astronautica*, Vol. 72, 2012, pp. 108–120. https://doi.org/10.1016/j.actaastro.2011.09.011.
- [15] Betts, J. T., "Optimal low-thrust orbit transfers with eclipsing," *Optimal Control Applications and Methods*, Vol. 36, No. 2, 2014, pp. 218–240. https://doi.org/10.1002/oca.2111

- [16] Graham, K. F. and Rao, A. V., "Minimum-Time Trajectory Optimization of Low-Thrust Earth-Orbit Transfers with Eclipsing," *Journal of Spacecraft and Rockets*, Vol. 53, No. 2, March-April 2016, pp. 289–303. https://doi.org/10.2514/1.A33416.
- [17] Lee, D., "Minimum-Fuel Planar Earth-to-Mars Low-Thrust Trajectories Using Bang-Bang Control," 2021. https://www.preprints.org/manuscript/202109.0226/v1.
- [18] Morante, D., Rivo, M. S., and Soler, M., "A Survey on Low-Thrust Trajectory Optimization Approaches," *Aerospace*, Vol. 8, No. 3, 2021, pp. 88(1)-88(39). https://doi.org/10.3390/aerospace8030088
- [19] Spencer, D. B., An analytical solution method for near-optimal, continuous-thrust orbit transfers, Ph.D. thesis, University of Colorado at Boulder, 1994.
- [20] Pager, E. R. and Rao, A. V., "Method for solving bang-bang and singular optimal control problems using adaptive Radau collocation," *Computational Optimization and Applications*, Vol. 81, No. 3, 2022, pp. 857–887. https://doi.org/10.1007/s10589--022--00350--6.
- [21] Patterson, M. A. and Rao, A. V., "GPOPS-II: A MATLAB Software for Solving Multiple-Phase Optimal Control Problems Using hp-Adaptive Gaussian Quadrature Collocation Methods and Sparse Nonlinear Programming," *ACM Transactions on Mathematical Software*, Vol. 41, No. 1, 2014, pp. 1:1–1:37. https://doi.org/10.1145/2558904.
- [22] NASA, "Modified Equinoctial Elements," 2005. https://spsweb.fltops.jpl.nasa.gov/portaldataops/mpg/MPG_Docs/Source%20Docs/EquinoctalElements-modified.pdf.
- [23] Betts, J. T., Practical Methods for Optimal Control and Estimation Using Nonlinear Programming, Society for Industrial and Applied Mathematics, 2010. https://doi.org/10.1137/1.9780898718577.
- [24] Graham, K. F. and Rao, A. V., "Minimum-Time Trajectory Optimization of Multiple Revolution Low-Thrust Earth-Orbit Transfers," *Journal of Spacecraft and Rockets*, Vol. 52, No. 3, 2015, pp. 711–727. https://doi.org/10.2514/1.a33187.
- [25] Biegler, L. T. and Zavala, V. M., "Large-Scale Nonlinear Programming Using IPOPT: An Integrating Framework for Enterprise-Wide Dynamic Optimization," Computers and Chemical Engineering, Vol. 33, No. 3, 2009, pp. 575–582. https://doi.org/10.1016/j.compchemeng. 2008.08.006.
- [26] Weinstein, M. J. and Rao, A. V., "Algorithm 984: ADiGator, a Toolbox for the Algorithmic Differentiation of Mathematical Functions in MATLAB Using Source Transformation via Operator Overloading," *ACM Transactions on Mathematical Software*, Vol. 44, No. 2, 2017, pp. 21:1–21:25. https://doi.org/10.1145/3104990.
- [27] Liu, F., Hager, W. W., and Rao, A. V., "Adaptive Mesh Refinement Method for Optimal Control Using Decay Rates of Legendre Polynomial Coefficients," *IEEE Transactions on Control System Technology*, Vol. 26, No. 4, 2018, pp. 1475–1483. https://doi.org/10.1109/TCST. 2017.2702122.
- [28] Garg, D., Patterson, M. A., Hager, W. W., Rao, A. V., Benson, D. A., and Huntington, G. T., "A Unified Framework for the Numerical Solution of Optimal Control Problems Using Pseudospectral Methods," *Automatica*, Vol. 46, No. 11, November 2010, pp. 1843–1851. https://doi.org/10.1016/j.automatica.2010.06.048.

- [29] Garg, D., Hager, W. W., and Rao, A. V., "Pseudospectral Methods for Solving Infinite-Horizon Optimal Control Problems," *Automatica*, Vol. 47, No. 4, April 2011, pp. 829–837. https://doi.org/10.1016/j.automatica.2011.01.085.
- [30] Garg, D., Patterson, M. A., Darby, C. L., Francolin, C., Huntington, G. T., Hager, W. W., and Rao, A. V., "Direct Trajectory Optimization and Costate Estimation of Finite-Horizon and Infinite-Horizon Optimal Control Problems via a Radau Pseudospectral Method," Computational Optimization and Applications, Vol. 49, No. 2, June 2011, pp. 335–358. http://dx.doi.org/10.1007/s10589--009--9291--0.
- [31] Kameswaran, S. and Biegler, L. T., "Convergence Rates for Direct Transcription of Optimal Control Problems Using Collocation at Radau Points," Computational Optimization and Applications, Vol. 41, No. 1, 2008, pp. 81–126. https://doi.org/10.1007/s10589--007--9098--9.
- [32] Patterson, M. A., Hager, W. W., and Rao, A. V., "A ph Mesh Refinement Method for Optimal Control," *Optimal Control Applications and Methods*, Vol. 36, No. 4, 2014, pp. 398–421. https://doi.org/10.1002/oca.2114.